An Event Database for Rotational Seismology

by Johannes Salvermoser, Céline Hadziioannou, Sarah Hable, Lion Krischer, Bryant Chow, Catalina Ramos, Joachim Wassermann, Ulrich Schreiber, André Gebauer, and Heiner Igel

ABSTRACT

We introduce a new event database for rotational seismology. The rotational seismology website (see Data and Resources) grants access to 17,000+ processed global earthquakes starting from 2007. For each event, it offers waveform and processed plots for the seismometer station at Wettzell and its vertical-component ring laser (G-Ring), as well as extensive metrics (e.g., peak amplitudes, signal-to-noise ratios). Tutorials and illustrated processing guidelines are available and ready to be applied to other data sets. The database strives to promote the use of joint rotational and translational ground-motion data demonstrating their potential for characterizing seismic wavefields.

INTRODUCTION

Seismology has been dominated by one type of observation: translational ground motions (usually measured as three orthogonal components: north–south, east–west, and vertical). In the past two decades, due to the emerging ring laser technology and its evolution toward higher sensitivities (Stedman, 1997; Schreiber and Wells, 2013) for geodetic applications, rotational ground motions have become available as a new observable in seismology. Aki and Richards (1980, 2002) pointed out that, to reconstruct complete ground motions, the rotational components should also be observed.

In this regard, McLeod *et al.* (1998) and Pancha *et al.* (2000) showed that vertical rotation rate and transverse acceleration are in phase, and Igel *et al.* (2005, 2007) and Kurrle *et al.* (2010) found that amplitude ratios of these measurements at a single point enable the estimation of dispersion curves of Love waves generated by (teleseismic) earthquakes.

Igel *et al.* (2007) additionally presented a straight-forward approach to infer the source direction (= back azimuth) from collocated broadband seismometer and ring laser recordings using a cross-correlation grid search.

The presented event database is the first of its kind and has two main intentions:

1. to make rotation data publicly available to promote its usage and significance for seismological applications. To this end, the database contains various plots and parameters for each event.
2. to demonstrate how rotational waveforms (e.g., vertical-component rotation rates from the Wettzell G-Ring) can be acquired and processed. For this purpose, we provide interactive tutorials in the form of open-source Jupyter notebooks (Pérez and Granger, 2007) which document the basic processing, as used for the database entries, while teaching helpful background information. The Python-based notebooks use routines from the well-known ObsPy library (Megies *et al.*, 2011; Krischer *et al.*, 2015) and can also be accessed through the recently initiate Jupyter notebook library for seismology (see Data and Resources).

At the time of writing (December, 2016), the database contains recordings from the Wettzell Geodetic Observatory in southeast Germany (Fig. 1a) and recent recordings from the first deep underground ring laser in the Gran Sasso massif in central Italy (Ortolan *et al.*, 2016; Simonelli *et al.*, 2016). The $4\ \mathrm{m} \times 4\ \mathrm{m}$ G-Ring laser (Fig. 1b) located in Wettzell is an interferometer, which measures the Sagnac frequency of two counter-propagating laser beams. Rotations of the instrument cause different lengths of both laser beam paths. The resulting beating is the so-called Sagnac frequency which is directly proportional to the interferometer's rotation rate (Stedman, 1997) around a perpendicular axis. The G-ring yields a very high resolution with a self-noise level around the vertical axis of $\approx 60 \times 10^{-14} (\mathrm{rad/s})\mathrm{Hz}^{-\frac{1}{2}}$ before May 2009 and $12 \times 10^{-14} (\mathrm{rad/s})\mathrm{Hz}^{-\frac{1}{2}}$ since May 2009, when the mirrors in the four corners of the ring laser were replaced to reach higher reflectivity (Schreiber and Wells, 2013). The achieved resolution is sufficient to record even smaller ($M_\mathrm{w} < 6$) teleseismic events at reasonable signal-to-noise ratios (SNRs) as well as Earth's free oscillations (Igel *et al.*, 2011) and ocean-generated noise (Hadziioannou *et al.*, 2012). Translational ground motions are measured with a collocated (distance ≈ 250 m) Streckeisen STS-2 broadband seismometer, the WET station of the German regional seismic network (GRSN). More than 17,000 events recorded at this station have been processed (see Fig. 2). The database is accessible via the website of the International Working Group on Rotational Seismology (see Data and Resources).

doi: 10.1785/0220160184

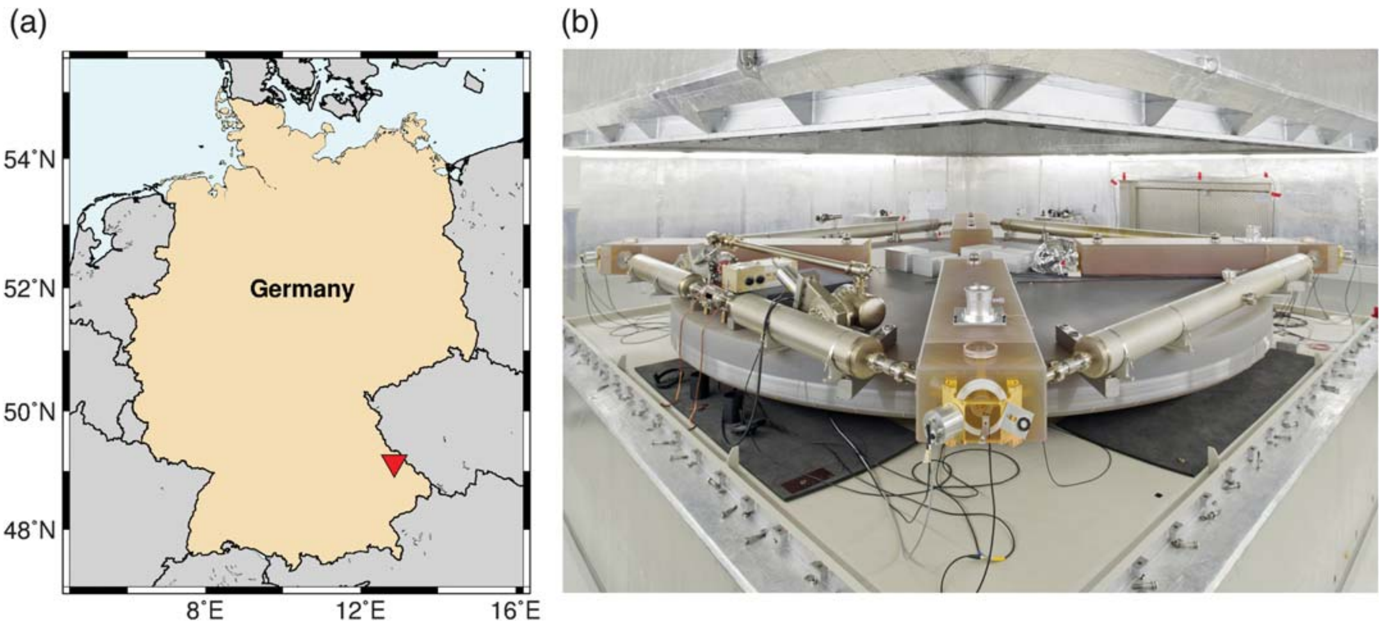

▲ **Figure 1.** (a) Location of the G-Ring laser and the collocated seismic station WET, indicated by the red triangle. (b) Picture of the G-Ring laser.

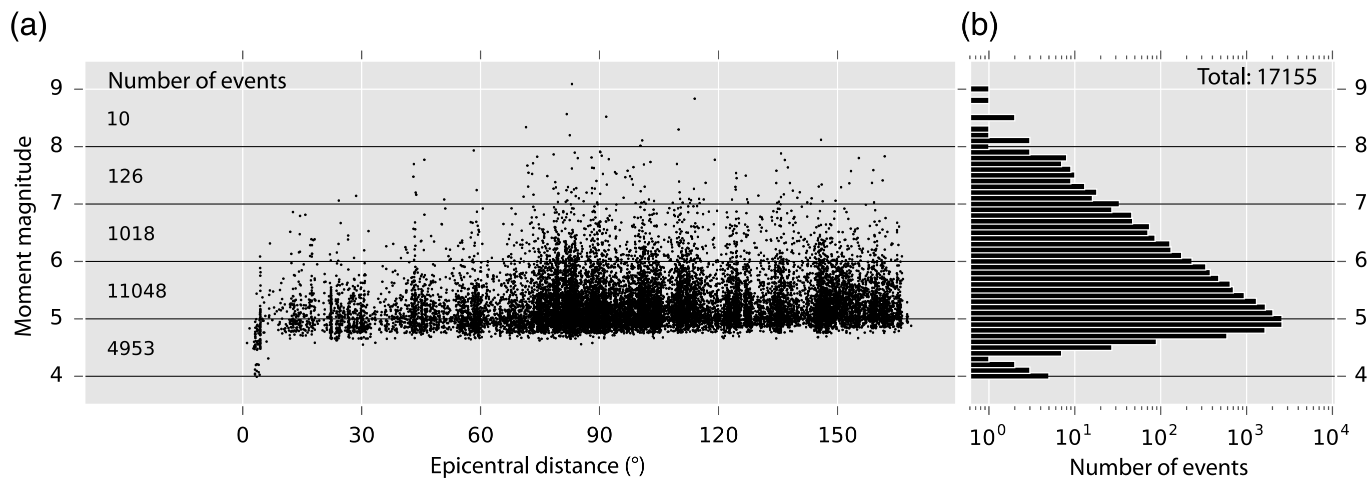

▲ **Figure 2.** (a) Distribution of the processed events from July 2007 to July 2016 by distance and magnitude and (b) number of events per magnitude in 0.1 steps. Events are provided by the Global Centroid Moment Tensor (Global CMT) catalog ($M \geq 4.5$) and local events ($M < 4.5$) are provided by the International Seismological Centre catalog.

WEB INTERFACE

The website provides the visitor with a graphical user interface of the database as well as additional information and links to topic-related projects (see Fig. 3).

Upon defining query parameters (time period, magnitude, depth, latitude and longitude, waveform coherence, peak rotation rate, and SNR), the user can choose between a downloadable QuakeML catalog (Wyss *et al.*, 2004) and a map representation of the specified available event catalog. On the zoomable world map, the earthquake event markers are sized and colored according to the earthquake's moment magnitude and source depth, respectively. This is intended to help find the desired event more quickly. By clicking on the event markers, a pop-up menu opens yielding a short description of the event by means of source time, magnitude, and depth. The menu also contains links to a couple of plots for the automatically processed waveform data of rotational and translational ground motions. These plots display the following:

1. event background information (location, time, etc.);
2. waveform comparison for four different time windows;
3. parameter estimation: Love-wave phase velocity (Fig. 4), back azimuth (Fig. 5); and
4. *P*-coda analysis.

Finally, the menu links to a metadata parameter file in the JavaScript Object Notation (JSON) format. This file contains

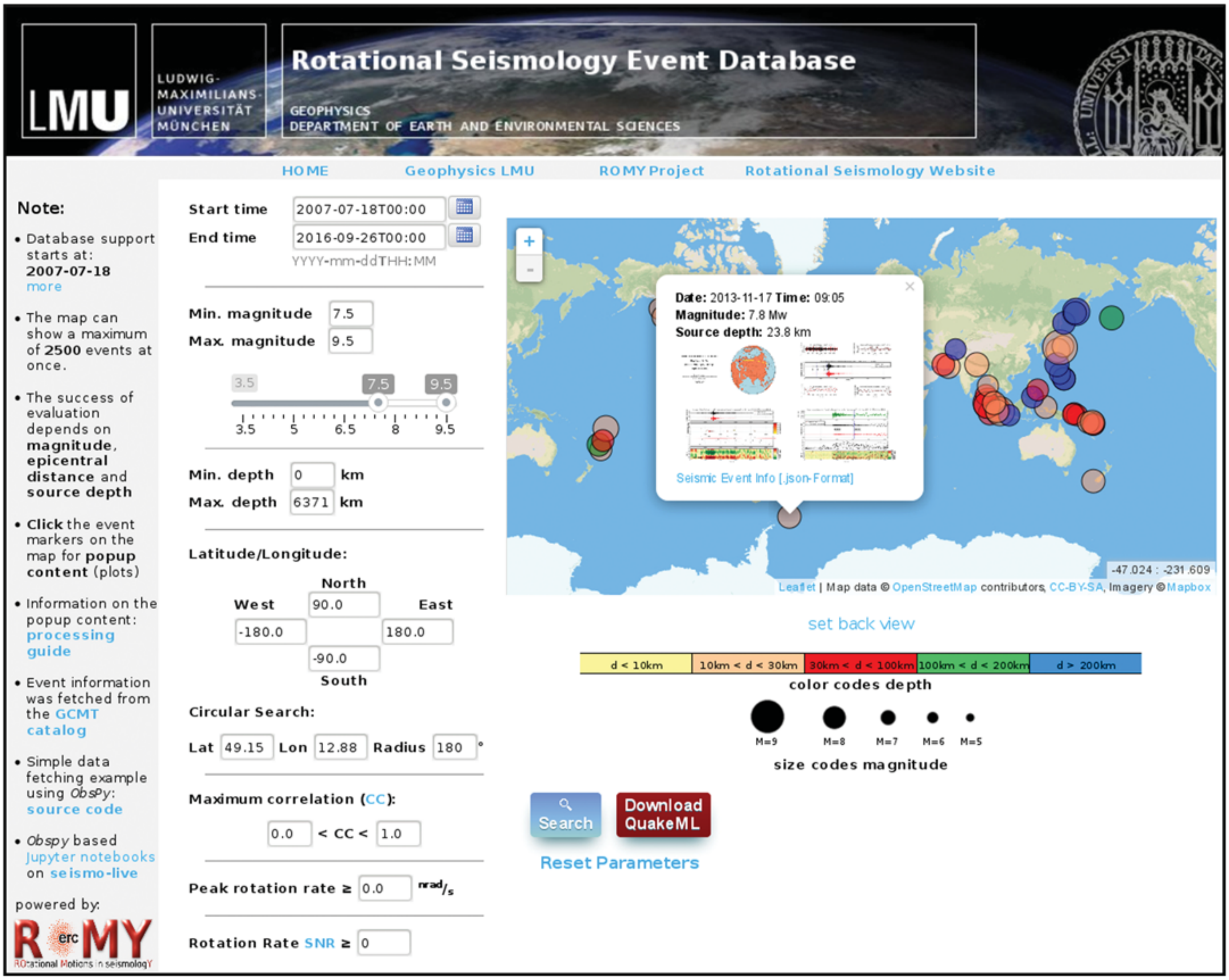

▲ **Figure 3.** Web view of the event database for rotational seismology. The left column comprises a collection of background information and links to source code snippets and tutorials. A query application allows the user to specify parameters to confine the requested event catalog. The Search option then plots the events on a map, whereas the Download QuakeML option allows the user to save the specified event catalog, including the additionally calculated rotation-specific metrics. The website information is available in Data and Resources.

all event and data fetching information and most importantly, the calculated parameters such as peak values (displacement, acceleration, rotation rate, correlation), SNRs, mean phase velocities and standard deviations, and estimated and theoretical back azimuths. These parameters are also part of the QuakeML catalog that can also be requested via standard Federation of Digital Seismograph Networks (FDSN) webservice.

An additional option to obtain event catalogs are http requests (e.g., see Data and Resources) which are described in an application.wadl. The Web Application Description Language (WADL) is an xml-formatted description for http-based webservice requests that contain parameter details and a functional catalog request example.

To make the processing and the plots reproducible, we include a downloadable processing guide and example code snippets on the database website. Additionally, Jupyter notebooks provided on this website interactively explain the processing steps from data download over instrument correction to phase velocity and back-azimuth estimation.

PROCESSING

In the following sections, we illustrate joint processing steps carried out on the collocated translational and rotational ground motions for each seismic event in the catalog.

Preprocessing

The event database is automatically updated on a daily basis. Scripts are fed by quick centroid moment tensor (CMT) solutions provided by the Global CMT catalog (Dziewoński *et al.*, 1981; Ekström *et al.*, 2012) and updated to the proper solutions once they are available. This catalog contains global

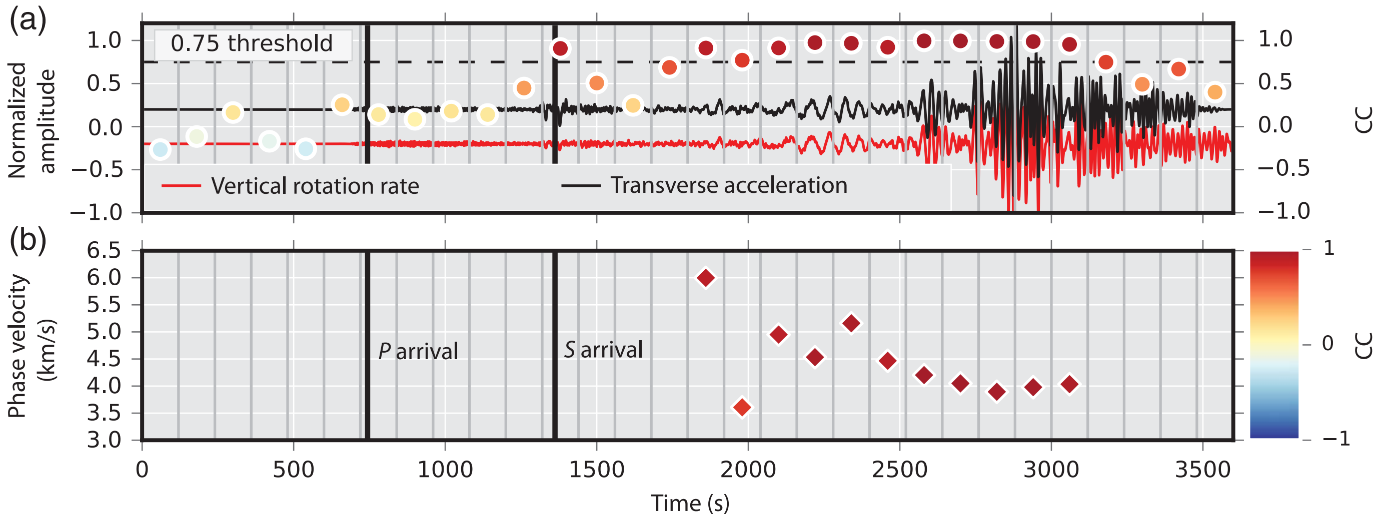

▲ **Figure 4.** Visualization of the sliding window phase velocity estimation for the M_w 9.0 Tohoku earthquake on 11 March 2011. For each of the time windows (120 s), a cross correlation is performed between vertical rotation rate and transverse acceleration (both low-pass filtered with a cutoff frequency of 1 Hz), depicted in (a). In (b), we estimate phase velocities for windows associated with correlation coefficients (CCs) larger than 0.75 and after the *S* phases.

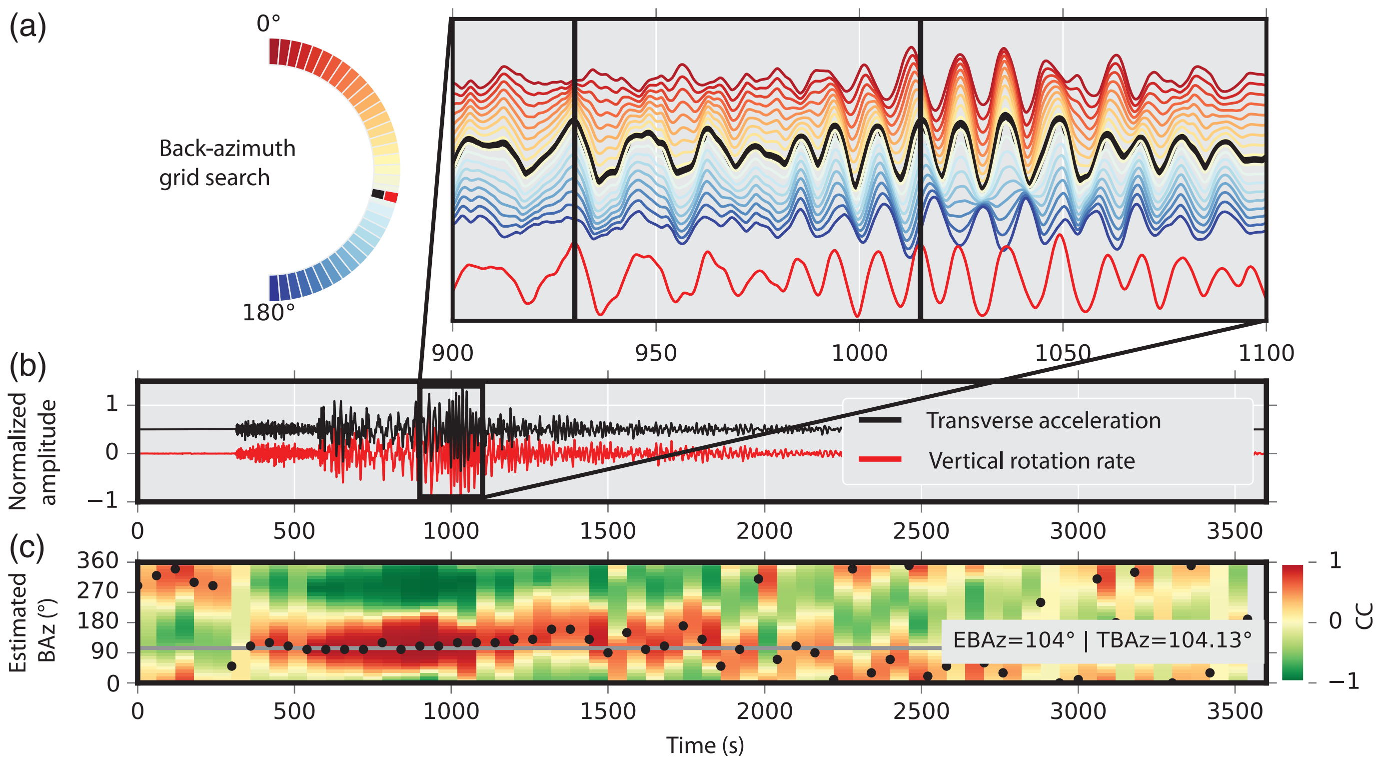

▲ **Figure 5.** Illustration of the back-azimuth estimation workflow at the example of the M_w 7.1 Turkey earthquake on 23 October 2011. (a) The grid-search algorithm loops through all possible source directions (red to blue) in 1° steps, cross correlating the two traces of transverse acceleration and vertical rotation rate (again low-pass filtered with $f_{cutoff} = 1$ Hz) shown in (b). In (c) for each time window, the BAz value related to maximum correlation is displayed as a black dot. Here, red color displays correlation, whereas green is anticorrelation of the traces for the specific BAz angle. Estimated (EBAz) and theoretical back azimuth (TBAz) are indicated by the gray solid line.

Table 1
Preprocessing Parameters

	Distance Range	Low-Pass Cutoff (Hz)	Cross-Correlation Window Length (s)	Microseism Bandstop (s)
Close	$0° \le d < 3°$	4	3	–
Local	$3° \le d \le 10°$	2	5	–
Tele	$d > 10°$	1	120	5–12

earthquake events featuring moment magnitudes $M_w \ge 4.5$. In addition to that, we provide smaller ($M_w < 4.5$) local and close events ($< 10°$ epicentral distance; compare with Table 1) using solutions of the International Seismological Centre (ISC, 2016; Di Giacomo *et al.*, 2014).

After fetching the event information (origin time, epicenter, depth, etc.), ring laser and collocated seismometer waveforms are downloaded from the GRSN data center. The preprocessing of the downloaded seismic data streams is determined by the epicentral distance (compare with Table 1).

The procedure starts with the removal of the seismometer's impulse response to convert to ground acceleration (nm/s^2) for the translational measurements and the scaling of the ring laser's rotation rate measurements to nrad/s. The traces are low-pass filtered to decrease the impact of high-frequency body waves and the ambient cultural noise. Furthermore, for teleseismic events, a bandstop-filter (5–12 s) is applied to reduce the effect of the secondary microseism (≈7 s period) which is more prominent than the primary microseism (Hadziioannou *et al.*, 2012) and can cause shifts in our back-azimuth estimation, especially for mid- to south-Atlantic events for the case of the Wettzell station location.

To determine the theoretical arrival times for the *P*- and *S*-wave windows, we run the ObsPy-tauP (Crotwell *et al.*, 1999) routine with the IASP91 model (Kennett and Engdahl, 1991). For the surface waves, arrivals are based on the corresponding IASP91 surface-wave travel times. The processing of phase velocity and back-azimuth estimation is described in the corresponding subsections below. It is notable that for the *P*-coda analysis, shorter time windows (local: 2 s; teleseismic: 5 s) are used for the cross-correlation analysis to show that there is a (weak) signal of *P*- or *SV*-converted *SH* waves in the high-frequency *P* coda and thus before the theoretical *S*-wave arrival (Pham *et al.*, 2009).

Love-Wave Phase Velocity Estimation

To derive Love-wave phase velocities, the observed amplitudes of rotational and preprocessed translational signals are combined (Igel *et al.*, 2005). Under the assumption of a transversely polarized plane wave, the vertical rotation rate $\dot{\Omega}_z$ and transverse acceleration a_t are in phase and the amplitudes are related by

$$\frac{a_t}{\dot{\Omega}_z} = -2c, \qquad (1)$$

in which c is the apparent horizontal phase velocity. In a first step, we therefore rotate the horizontal acceleration components (northeast) in the source–receiver plane to radial–transverse by the theoretical back azimuth (BAz) to optimize the phase match with the vertical rotation rate. The transverse acceleration and vertical rotation rate traces are then divided into sliding windows of equal size, depending on the epicentral distance of the event (see Table 1). For each of these windows, a zero-lag normalized cross-correlation analysis is applied to a_t and $\dot{\Omega}_z$ to check the coherence between the two waveforms (Fig. 4a). The resulting cross-correlation coefficient (CC) is used as a quality criterion for the determination of the phase velocities. For windows with CC > 0.75, the horizontal phase velocity c is estimated by inserting peak values of a_t and $\dot{\Omega}_z$ into equation (1) (Fig. 4b). For broadband traces and high waveform coherence (= high-quality signal), we obtain an impression of the dispersive behavior of fundamental-mode Love waves immediately by looking at the temporal evolution of the phase velocity: the dominant frequency of Love waves increases with time, whereas phase velocities decrease. This behavior can be seen in Figure 4 after the onset of Love waves around 2200 s.

Back-Azimuth Estimation

Similar to the phase velocity estimation following the approach by Igel *et al.* (2007), we investigate sliding windows throughout the signal to determine the evolution of the signal source direction. The traces are split into windows according to Table 1. For each window, we estimate the direction of the signal in two preprocessed traces (vertical rotation rate and transverse acceleration) employing a grid-search optimization algorithm.

This search loops through all possible back-azimuth directions (0°–360°) in 1° steps, rotates the horizontal-component acceleration (northeast) by the specified BAz angle, and then cross correlates it with the vertical rotation rate. The process is illustrated in Figure 5a in which a color range is assigned to different BAz rotation angles. The CCs show a maximum for a rotation from northeast to radial–transverse, which is equivalent to rotating in the direction of the strongest signal source (transverse acceleration [black] and vertical rotation rate [red] are in phase).

Only windows reaching 90% correlation after rotation are considered in the estimation of the final BAz value, which is the average of the associated (CC > 0.9) BAz results (solid line in Fig. 5c). Larger discrepancies between the theoretical and estimated BAz in combination with higher CCs on the estimated BAz side may indicate deviations of the Love wavepath in the source-receiver plane, or effects due to anisotropy, or scattering.

CONCLUSIONS

In the light of the rapidly improving rotation sensor technology and prospects of portable broadband rotation sensors for seismology (Bernauer *et al.*, 2016; see Data and Resources), we intend to promote the processing and use of rotational motion recordings by providing ready-to-use processing results as well as illustrating real data processing examples using ObsPy. Event parameters and waveform plots of more than 17,000 earthquakes since 2007 can be downloaded and used for statistical analysis. This, for example, allows investigating the peak rotational ground motions as a function of magnitude and distance and the analysis of azimuthal effects on the wavefield.

In the future, we plan on including data of additional rotational sensors allowing interstation comparison. As soon as their continuous rotational motion recordings are available, we will include ring lasers such as the ones located at the observatories of Piñon Flat (U.S.A., GEOsensor; Schreiber, Velikoseltsev, *et al.*, 2003), Christchurch (New Zealand; Schreiber, Klügel, *et al.*, 2003) and the four-component ring laser in Fürstenfeldbruck (Germany; Rotational Motions in Seismology [ROMY]) to be installed in 2017. We also plan to integrate measurements of array derived rotations and portable rotation sensors as soon as high-quality data are available.

DATA AND RESOURCES

The Global Centroid Moment Tensor (Global CMT) Project database was searched using www.globalcmt.org (last accessed August 2015). The rotational seismology website is available at www.rotational-seismology.org and http://www.rotational-seismology.org/data (both last accessed March 2017); Jupyter notebook library for seismology is at www.seismo-live.org (last accessed March 2017); and portable broadband rotation sensors for seismology is at www.blueseis.com (last accessed March 2017). An additional option to obtain event catalogs are http requests, for example: WEBSITE_URL/fdsnws/event/1/query?minmag=8&maxdepth=25&mincor=0.8 (last accessed March 2017).

ACKNOWLEDGMENTS

This work was supported by the European Research Council (ERC) Advanced Grant "ROMY." Additional support was provided by the German Research Foundation (DFG) for the HA7019/1-1 Emmy-Noether Progamme Grant (C. H.) and the Schr645/6-1 Grant (A. G.). We also acknowledge support from the EU-funded European Plate Observatory System (EPOS) Project.

REFERENCES

Aki, K., and P. G. Richards (1980). *Quantitative Seismology*, First Ed., University Science Books, San Francisco, California.

Aki, K., and P. G. Richards (2002). *Quantitative Seismology*, Second Ed., University Science Books, Sausalito, California.

Bernauer, F., J. Wassermann, F. Guattari, and H. Igel (2016). Portable sensor technology for rotational ground motions, presented at the *EGU General Assembly*, Vienna, Austria, 21 April 2016, Paper Number SM7.2/G6.2.

Crotwell, H., T. Owens, and J. Ritsema (1999). The TauP toolkit: Flexible seismic travel-time and ray-path utilities, *Seismol. Res. Lett.* **70,** no. 2, 154–160.

Di Giacomo, D., D. Storchak, N. Safronova, P. Ozgo, J. Harris, R. Verney, and I. Bondár (2014). A new ISC service: The bibliography of seismic events, *Seismol. Res. Lett.* **85,** no. 2, 354–360.

Dziewoński, A. M., T.-A. Chou, and J. H. Woodhouse (1981). Determination of earthquake source parameters from waveform data for studies of global and regional seismicity, *J. Geophys. Res.* **86,** no. B4, 2825–2852.

Ekström, G., M. Nettles, and A. Dziewoński (2012). The global CMT project 2004–2010: Centroid-moment tensors for 13,017 earthquakes, *Phys. Earth Planet. In.* **200/201,** 1–9.

Hadziioannou, C., P. Gaebler, U. Schreiber, J. Wassermann, and H. Igel (2012). Examining ambient noise using colocated measurements of rotational and translational motion, *J. Seismol.* **16,** no. 4, 787–796.

Igel, H., A. Cochard, J. Wassermann, A. Flaws, U. Schreiber, A. Velikoseltsev, and N. Pham Dinh (2007). Broad-band observations of earthquake-induced rotational ground motions, *Geophys. J. Int.* **168,** no. 1, 182–196.

Igel, H., M.-F. Nader, D. Kurrle, A. M. G. Ferreira, J. Wassermann, and K. U. Schreiber (2011). Observations of Earth's toroidal free oscillations with a rotation sensor: The 2011 magnitude 9.0 Tohoku-Oki earthquake, *Geophys. Res. Lett.* **38,** L21303, doi: 10.1029/2011GL049045.

Igel, H., U. Schreiber, A. Flaws, B. Schuberth, A. Velikoseltsev, and A. Cochard (2005). Rotational motions induced by the M 8.1 Tokachi-Oki earthquake, September 25, 2003, *Geophys. Res. Lett.* **32,** L08309, doi: 10.1029/2004GL022336.

International Seismological Centre (ISC) (2016). *On-line Event Bibliography*, International Seismological Centre, Thatcham, United Kingdom, available at http://www.isc.ac.uk/event_bibliography (last accessed March 2017).

Kennett, B. L. N., and E. R. Engdahl (1991). Traveltimes for global earthquake location and phase identification, *Geophys. J. Int.* **105,** no. 2, 429–465.

Krischer, L., T. Megies, R. Barsch, M. Beyreuther, T. Lecocq, C. Caudron, and J. Wassermann (2015). ObsPy: A bridge for seismology into the scientific Python ecosystem, *Comput. Sci. Discov.* **8,** no. 1, 014003.

Kurrle, D., H. Igel, A. M. G. Ferreira, J. Wassermann, and U. Schreiber (2010). Can we estimate local love wave dispersion properties from collocated amplitude measurements of translations and rotations? *Geophys. Res. Lett.* **37,** L04307, doi: 10.1029/2009GL042215.

McLeod, D. P., G. E. Stedman, T. H. Webb, and U. Schreiber (1998). Comparison of standard and ring laser rotational seismograms, *Bull. Seismol. Soc. Am.* **88,** no. 6, 1495–1503.

Megies, T., M. Beyreuther, R. Barsch, L. Krischer, and J. Wassermann (2011). ObsPy—What can it do for data centers and observatories? *Ann. Geophys.* **54,** no. 1, doi: 10.4401/ag-4838.

Ortolan, A., J. Belfi, F. Bosi, A. D. Virgilio, N. Beverini, G. Carelli, E. Maccioni, R. Santagata, A. Simonelli, A. Beghi, *et al.* (2016). The GINGER project and status of the GINGERino prototype at LNGS, *J. Phys. Conf.* **718,** no. 7, 072003.

Pancha, A., T. Webb, G. Stedman, D. McLeod, and K. Schreiber (2000). Ring laser detection of rotations from teleseismic waves, *Geophys. Res. Lett.* **27,** no. 21, 3553–3556.

Pham, N. D., H. Igel, J. Wassermann, M. Käser, J. de la Puente, and U. Schreiber (2009). Observations and modeling of rotational signals in the P coda: Constraints on crustal scattering, *Bull. Seismol. Soc. Am.* **99,** no. 2B, 1315–1332.

Pérez, F., and B. E. Granger (2007). IPython: A system for interactive scientific computing, *Comput. Sci. Eng.* **9,** no. 3, 21–29.

Schreiber, K. U., and J.-P. R. Wells (2013). Invited review article: Large ring lasers for rotation sensing, *Rev. Sci. Instrum.* **84,** no. 4, doi: 10.1063/1.4798216.

Schreiber, K. U., T. Klügel, and G. E. Stedman (2003). Earth tide and tilt detection by a ring laser gyroscope, *J. Geophys. Res.* **108,** no. B2, 2132.
Schreiber, K. U., A. Velikoseltsev, H. Igel, A. Cochard, A. Flaws, W. Drewitz, and F. Müller (2003). The GEOsensor: A new instrument for seismology, *GEO-TECHNOLOGIEN Science Report 3*, 12–13.
Simonelli, A., J. Belfi, N. Beverini, G. Carelli, A. Di Virgilio, E. Maccioni, G. De Luca, and G. Saccorotti (2016). *First Deep Underground Observation of Rotational Signals from an Earthquake at Teleseismic Distance Using a Large Ring Laser Gyroscope*, available at https://arxiv.org/abs/1601.05960 (last accessed March 2017).
Stedman, G. E. (1997). Ring-laser tests of fundamental physics and geophysics, *Rep. Progr. Phys.* **60,** no. 6, 615.
Wyss, A., D. Schorlemmer, S. Maraini, M. Baer, and S. Wiemer (2004). QuakeML—An XML Schema for Seismology, *Eos Trans. AGU* **85,** no. 47 (Fall Meet. Suppl.), Abstract S21A–0272.

Johannes Salvermoser
Céline Hadziioannou[1]
Sarah Hable
Lion Krischer
Bryant Chow
Joachim Wassermann
André Gebauer
Heiner Igel
Department of Earth and Environmental Sciences
Ludwig-Maximilians-University Munich
Theresienstrasse 41
D-80333 Munich, Germany
heiner.igel@lmu.de

Catalina Ramos
Deutsches GeoForschungszentrum GFZ
Section Geophysical Deep Sounding
Telegrafenberg
D-14473 Potsdam, Germany

Ulrich Schreiber
Forschungseinrichtung Satellitengeodäsie
Technical University Munich
Fundamentalstation Wettzell, Sackenriederstrasse 25
D-93444 Kötzting, Germany

Published Online 29 March 2017

[1] Now at Institute for Geophysics, University of Hamburg, Bundesstrasse 55, D-20146 Hamburg, Germany.